Biointerface Research in Applied Chemistry
Open-Access Journal (ISSN: 2069-5837)

Article
Volume 13, Issue 6, 2023, 531
https://doi.org/10.33263/BRIAC136.531

Synthesis, Spectral Characterisation of Novel Azo–Dye 4-((E)-(2-Hydroxy-3-Methoxy-5-((E)-Thiazol-2-Yldiazenyl)Benzylidene)Amino)-1,5-Dimethyl-2-Phenyl-1H-Pyrazol-3(2H)-One and its Transition Metal Complexes; Differential Pulse Voltammetric Detection of Nitrite and its Biological Activities

Vasantakumaranaik Narayanapura Krishnanaik [1], Ganganaik Krishnamurthy, [1,*], Malathesh Pari [1], Nagaraju Venugopal [1], Nanjundaswamy Ranjitha [1], Nagaraja Naik [2]

[1] Department of Chemistry, Sahyadri Science College, Kuvempu University, Shivamogga-577203, Karnataka, India; vasanthnaiknk77@gmail.com (V.N.K.); gkmnaiksahyadri@gmail.com (G.K.); malathshpari@gmail.com (M.P.); venuchavan9@gmail.com (N.V.); ranjuranju.n994@gmail.com (N.R.);
[2] Department of chemistry, University of Mysore-570005, Mysore, Karnataka, India; drnaikchem@gmail.com (N.N.);
* Correspondence: gkmnaiksahyadri@gmail.com (G.K.);

Scopus Author ID 36190957700
Received: 3.10.2022; Accepted: 19.11.2022; Published: 5.02.2023

Abstract: The novel azo-azomethine 4-((E)-(2-hydroxy-3-methoxy-5-((E)-thiazol-2-yldiazenyl)benzylidene)amino)-1,5-dimethyl-2-phenyl-1H-pyrazol-3(2H)-one (HTDP) and its Cu(II), Co(II) and Ni(II) complexes were synthesized, and their structure was confirmed by using physicochemical techniques. The spectrochemical data indicate that the synthesized ligand is tridentate in nature. The antimicrobial, anti-diabetes (A-DM), and anti-mycobacterium tuberculosis (M-TB) activities against ligands and their metal complexes were screened. The complexes exhibited enhanced bio-efficiency inhibitory results when compared to the HTDP. Excess nitrate poses harmful effects on the ecological system and causes the blue baby syndrome. The modified glassy carbon electrode prepared using $[Co(HTDP)_2]$ is used for electrochemical sensing of nitrate under different concentrations and displayed good electro-catalytic activity with long linear range (10-80 $\mu molL^{-1}$), sensitivity (0.172 $\mu A\mu M^{-1}\ cm^{-2}$) and the LOD (limit of detection) found to be 3.333 μML^{-1} in PBS (pH 7) Further, the prepared sensor has more stability and showed less pouling property.

Keywords: metal complexes; TGA; nitrate; cyclic voltammetry; DPV; antimicrobial; antidiabetic and anti-tuberculosis activities.

1. Introduction

The heterocyclic compounds with at least two different donor atoms, like sulfur and nitrogen, have been studied widely due to their various biological activities [1-3]. The Schiff base (R_1-C=N-R_2) compounds have a group-specific condensation reaction for aldehyde/ketone with an amine. Coordination of ligand to metal ions occurs via azomethine nitrogen. The heterocyclic donor elements and azomethine group increase the potential applications for therapeutic activities. The azo Schiff bases are color chromophoric which are used in the synthetic colorant in cosmetics, fabrication, natural health products, insecticides,

recording layers of DVD, CD, textile cilium, plastics, leather-fell, metal sheets, food, and toys, etc. [4-6]. The chelating ligands coordinating with metal ions exhibit enhanced physicochemical and catalytic behavior. The transition metal based-drugs with lesser toxicity can be used as target-specific activities with a wide range of potential therapeutic applications, including antimicrobial, anticancer, antidiabetic, and anti-tuberculosis.

Antidiabetic and anti-tuberculosis are chronic diseases and are very dangerous. Tuberculosis is a communicable disease and is a major cause of ill health by bacillus mycobacterium grows tuberculosis in people when sick. Due to cough, the virus spreads through the air and affects the lungs (pulmonary). Most people suffer from the hazards of TB and related diabetes. Due to their high sensitivity, the metal complexes exhibited electrochemical properties due to redox behavior [7-9]. Thus, the modified glassy carbon electrode prepared using a metal complex can determine the nitrite [10]. Nitrate is an essential trace element for animals and plants. It is produced in the environment by the nitrogen cycle, fertilizer, and decomposition of animal waste. It refers to –ONO group and is also called vasodilator medication. Medicine uses it to treat angina, cure ingredients, and preserve food. Excess nitrate causes harmful effects on the ecological system, water bodies, and especially on children (methemoglobinemia / blue baby syndrome).

Moreover, Befoul nitrate arising from muck has hazardous effects on the human living system [11-13]. Thus, the determination of nitrate is very important. Literature showed that cyclic voltammogram is a potential, sensitive, rapid, and reliable method for the detection of NO_2. This method is used to investigate the electrochemical feature of a substance in solution.

Our research group has synthesized N, S heterocycles, and its metal complexes and evaluated their anticancer activity and electrochemical studies. In continuation of our research work, we reported here the synthesis of a novel [4-((E)-(2-hydroxy-3-methoxy-5-((E)-thiazol-2-yldiazenyl)benzylidene)amino)-1,5-dimethyl-2-phenyl1H-pyrazol-3(2H)one], and its Cu(II), Co(II), Ni(II) complexes followed by evaluation of their biological activities as well as the electrochemical determination NO_2 have been carried out [13].

2. Materials and Methods

2.1. Source and instrumentations.

All the chemicals used were of analytical grade and purchased from Avra, Himedia, and Merck companies which were used without further purification. The melting point is determined by the digital melting point apparatus, electrothermal IA9100. The synthesized compounds were characterized by UV-Vis spectrophotometer in the range 200-800 nm using Systronics 119 model in DMF solvent. The elemental analysis was performed on a CHN analyzer Carlo Erba 1108 analyzer. The IR spectra were recorded using a KBr pellet in a Shimadzu FT-IR spectrophotometer in the range 4000–400 cm^{-1}. 1H NMR spectrum of the ligand was determined by BRUKER Ascend 400MHz FTNMR spectrometer using tetramethylsilane as an internal reference standard. The electrochemical analysis was done by CHI 620E analyzer Inc. made in the U.S.A. The powder XRD was recorded on powder x-ray diffraction facility code XRD POWDER100. Mass spectra of the compounds were determined on LC-MS water AQUITY-2777C mass spectrometer. The molar conductance measurement was conducted using an ELICO-CM82 conductivity meter. The magnetic moment of the complexes was noted at 28 °C by Gouy balance version 7550 using $Hg[Co(NCS)_4]$ as a

calibrant. The TGA of complexes was carried out on SII Exstar TG/DTA 6300 instrument from the laboratory temperature to 1000 °C with a scan rate of 10 °C/ min.

2.2. Synthesis of azo dye ligand (HTDP).

The ligand HTDP has been synthesized in two steps. The starting material was prepared using a diazonium salt solution and 2-hydroxy-3-methoxy benzaldehyde in the first step. The solution of diazonium salt was prepared by dissolving 3 mM/0.3g of 1,3-thiazole-2-amine in 10 mL of distilled water along with 5 mL of concentrated hydrochloric acid, which was maintained at 0-5 °C for 1 h and 4 mL of 3 mM/0.2g $NaNO_2$ solution was added dropwise in amine solution with continuous stirring. The obtained diazonium salt solution was added to a cold solution of 2-hydroxy-3-methoxy benzaldehyde (3 mM/0.46g) in basic media. The resulting solution was stirred for 1 h at the same temperature by maintaining pH 6-7. After completion of the reaction, the reaction solution was poured into ice-cold water. The solid product obtained was (2-hydroxy-3-methoxy-5-[(Z)-1,3-thiazol-2-yldiazenyl]benzaldehyde.

In the second step, (2-hydroxy-3-methoxy-5-[(Z)-1,3-thiazol-2-yldiazenyl]benzaldehyde (2 mM/0.6g) and 4-amino antipyrine (2 mM/0.5g) dissolved in 20 mL methanol. Acetic acid was added to the above solution's catalytic amount of (4 drops). The above mixture was stirred under reflux for 4 h. The progress of the reaction was monitored by TLC (ethyl acetate: petroleum ether, 4:6). After completion of the reaction; the solution was poured into ice-cold water to get [4-((E)-(2-hydroxy-3-methoxy-5-((E)-thiazol-2-yldiazenyl)benzylidene)amino)-1,5-dimethyl-2-phenyl1H-pyrazol-3(2H)one] (HTDP). The precipitate was filtered, washed with ethanol, and recrystallized from the methanol [13]. The synthetic route is presented in Scheme 1.

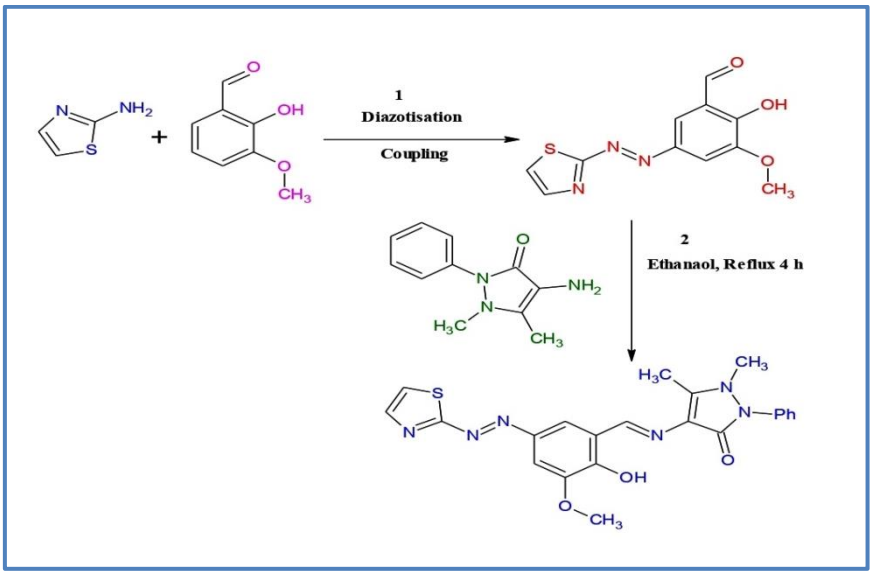

Scheme 1. [4-((E)-(2-hydroxy-3-methoxy-5-((E)-thiazol-2-yldiazenyl)benzylidene)amino)-1,5-dimethyl-2-phenyl1H-pyrazol-3(2H)one] (HTDP).

2.2.1. Synthesis of metal complexes.

All the complexes were prepared in the stoichiometric ratio 1:2 of metal: ligand. A solution of copper chloride was prepared in 20 mL methanol (1mM/0.15g) and added to the hot methanol solution of HTDP (2 mM/1g) with continuous stirring. The resulting solution was refluxed for 4 h in the temperature range of 50-60 °C. The solid precipitate was collected by filtration, washed several times with ethanol, rinsed with ethanol, then kept in a desiccator [13,

14]. A similar method was followed for preparing Co(II) and Ni(II) complexes by taking the solution of a respective metal chloride, as represented in Scheme 2. Yield is 75–80%.

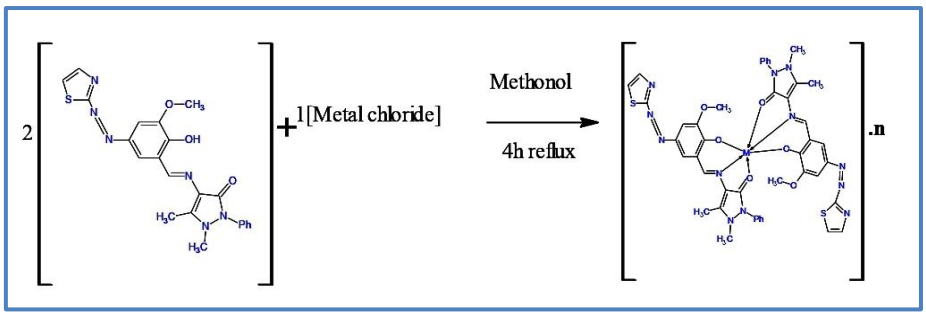

Scheme 2. Preparation of $[Cu(HTDP)_2]H_2O$, $[Co(HTDP)_2]$ and $[Ni(HTDP)_2]2H_2O$.

2.3. Electrochemistry instrumentation.

Nitrate detection has been performed by cyclic voltammetry. It consists of the 3-electrode system; the working electrode is a glassy carbon electrode (GCE), platinum as a counter electrode (PCE), and Ag/AgCl electrode as a reference electrode in the redox system. The GC electrode was wiped with alumina powder and washed properly with deionized water. Subsequently, 10 µL of $[Co(HTDP)_2]$ in DMF drop coated on the electrode surface area. This was used to detect nitrate in phosphate buffer (pH 7) solution [15, 16].

2.4. Biological evaluation.

2.4.1. Antimicrobial activities.

The antimicrobial activity of HTDP and their metal complexes screened against bacterial cultures of gram +ve *S. aureus* (MTCC-7443), gram –ve *E. coli* (MTCC-7410), *Shigella* (MTCC-1457) and *clostridium* (MTCC-11078). The fungal Cultures like *Aspergillus niger* (MTCC-1207) and *Fusarium* (MTCC-1372) were used for dual-culture agar well diffusion assay along with some modifications. A Petri plate was prepared using 20 mL of sterilized nutrient agar for bacterial, and potato dextrose agar media for fungal cultures were adjusted under aseptic conditions. The 100 µL of standardized test microbial was transferred by using an inoculum glass loop. Screening in various concentrations and 1 mg/mL were tested. Further, diluting the sample with DMSO was added to plates; after that, the plates were incubated under 37 ºC for one day. Chloramphenicol was considered standard for bacterial assay, and nystatin was used for the antifungal assay. The diameter of the inhibition zone was measured in millimeters (mm), and three repeated trials were taken to assess the strength of antibacterial activity [17, 18].

2.4.2. Antidiabitic study.

Inhibition of alpha-amylase enzyme was carried out according to the standard methods with a small modification. In a test tube, the reaction mixture containing 500 µL phosphate buffer (100 mM, pH 6.8), 100 µL α–amylase (2 U/mL), and 200 µL of extract of different concentrations of HTDP and its metal complexes from 25 to 100 µg was pre-incubated at 37 °C for 20 min. Then, the 200 µL of 1% soluble starch (100 mM phosphate buffer pH 6.8) was added as a substrate and incubated further at 37 °C for 30 min. 1 mL of the DNS color reagent was added and kept in a water bath for 10 min. The absorbance of the resulting mixture was

measured at 540 nm using a UV-Visible spectrophotometer. Acarbose (0.1–0.5 mg/mL) was used as a standard, and the experiment was executed in three replicates.

The percentage of Alpha-amylase inhibition was calculated using the equation is

$$= [AC - \frac{AE}{AC}] \times 100$$

AC: absorbance of control and AE: absorbance of extract [19, 20].

The dose efficiency IC_{50} value was calculated via standard Excel linear regression method by the average value of the zone inhibition result in various concentrations.

2.4.3. Anti-tuberculosis activity.

Mycobacterium tuberculosis MTCC 300, the culture was developed, and sub-cultured functioning Middle brook 7H10 [21, 22] with some of the modification was prepared well-mannered in the nutrient broth at 37 °C for 48 h for Anti-tuberculosis assay. The growth was noted down spectrophotometrically at 600 nm. The MIC assay was detected using a tetrazolium salt indicator, MTT (3-4,5-dimethylthiazol-2-yl-2,5-diphenyl tetrazolium bromide). The MIC assay took an aliquot of 25, 50, and 100 µL of 0.1 g/mL of the ligand and its metal complexes. MTT was pipetted into each well (40 µL at 0.2 mg/mL), and once growth control wells revealed a purple color following incubation at 37 °C for 1 h viable by the agent. The color formation indicated growth inhibition in the assay. An average of three repeated tests was taken to assess the strength of the activity. Chloramphenicol was considered a standard [23, 24]. The minimum inhibitory concentration IC_{50} value was evaluated by excels linear regression technique by the mean value of the activity in different concentrations region.

3. Result and Discussion

3.1. Characterization.

The reaction of an azo dye, HTDP, with metal chlorides produces the complexes of the formula $[Cu(HTDP)_2]H_2O$, $[Co(HTDP)_2]$ and $Ni(HTDP)_2]2H_2O$. The synthesized ligand and its complexes were characterized by various spectroscopic techniques. The prepared complexes are colored, crystalline solid, and stable toward air and moisture at the laboratory temperature. The complexes are insoluble in a common organic solvent but soluble in DMF and DMSO solvents. The molar conductance measurements of the complexes used in DMF (1×10^{-3} M) solution reported 18-29 Ω^{-1} cm^2 mol^{-1} indicating non-electrolytic nature [25]. The experimental, analytical data of HTDP and their metal complexes are reported in Table 1.

Table 1. Physical and analytical data of HTDP and its complexes.

Compounds	Color	Mol. wt	M.P in °C	Elemental analysis in (%) Cal				Λm Ω^{-1} cm^2 mol^{-1}
				C	H	N	M	
HTDP	Reddish brown	449.25	≥ 166	59.9 (58.8)	4.46 (4.45)	18.7 (18.7)		
$[Cu(HTDP)_2]H_2O$	Brick pink	976.5	≥ 177	54 (54)	4.9 (4.7)	17.2 (17.1)	6.4 (6.3)	24
$[Co(HTDP)_2]$	Bluish brown	953.9	≥ 204	55.4 (55.2)	3.9 (3.82)	17.6 (17.5)	5.6 (5.5)	29
$[Ni(HTDP)_2]2H_2O$	Dark red	989.3	≥ 179	53.3 (53.13)	4.2 (4.14)	16.9 (16.4)	5.8 (5.79)	19

3.2. ^1H NMR spectral data.

The newly synthesized HTDP has been characterized by ^1H NMR in DMSO-d_6 solvent at room temperature, and the spectrum is represented in Figure 1. The Ar-OH group proton

signal appeared as a singlet at 14.25 ppm, and the proton of azomethine group resonance appeared at 9.80 ppm (s, 1H, CH=N). The signals from aromatic protons appeared in the region 8.09-7.39 ppm (m, 9H, Ar-H), and methyl protons of the 4-aminoantypirine ring (s, 3H, C-CH_3) showed around 2.50 ppm. Another methyl group signal of N-CH_3 proton exhibited a singlet at 3.36 ppm. The methoxy group protons showed a singlet on 3.94 ppm (s, 3H, Ar-OCH_3) [25, 26].

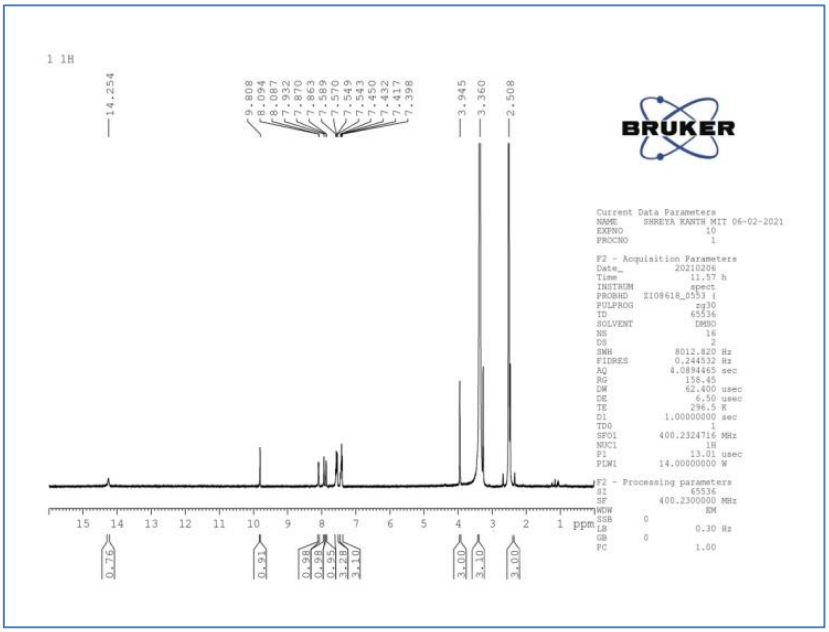

Figure 1. ^{1}H NMR spectrum of HTDP*3.3. Infrared spectra studies.*

The IR spectra of HTDP and their coordinated complexes are shown in Supplementary Figure S1, and the data are compiled in Table 2. The peak that appeared at 3002 cm^{-1} is due to C-H stretching, and the ν(C=N) of the azomethine group exhibited a signal at 1553 cm^{-1}. The ν(-C=O) stretching was obtained at 1601 cm^{-1}. The peaks of azomethine and carbonyl groups shifted to 30-40 cm^{-1} in their complexes due to the formation of ligand–metal coordination bonds. A band due to ν(OH) of ligand appeared at 3393 cm^{-1}, and this band is absent in the spectra of their complexes, indicating the elimination of hydrogen of the OH group; hence and it justified that the OH group is also involved in the coordination bond formation. Further, the complex formation is confirmed by the appearance bands around 480 cm^{-1} for ν(M-N), and ν(M-O) obtained at 580-690 cm^{-1}. The band due to ν(N=N) appeared at 1441 cm^{-1} in the spectrum of the uncoordinated ligand, and it appeared at the same position in their metal complexes, indicating the non-involvement of the N=N group in the coordination. Thus spectral results confirmed the tridentate nature of the ligand [27-29].

Table 2. FT-IR spectral data (cm^{-1}) of ligand and its metal complexes.

Compound	ν(–OH)	ν(Ar-CH)	ν(C=O)	ν(C=N)	(N=N)	ν(M-N)	ν(M-O)
HTDP	3393	3002	1601	1533	1441	-	-
$[Cu(HTDP)_2]H_2O$	-	3000	1582	1549	1447	457	581
$[Co(HTDP)_2]$	-	3001	1565	1519	1442	489	689
$[Ni(HTDP)_2]2H_2O$		3002	1586	1551	1443	486	673

3.4. UV-Visible studies.

The Uv-visible absorption bands of synthesized HTDP and their coordinated metal complexes were noted in the DMF solution. The free HTDP exhibited an absorption band at

22,727 cm^{-1}, which is ascribed to n→π* of the (–N=N–) group. Further, the absorption band due to the (–N=N–) group in all the metal complexes is shifted to a higher wavelength indicating coordination of the metal chlorides with the HTDP. The electronic absorption spectrum of $[Cu(HTDP)_2]H_2O$ showed two bands at 24,570, and 18518 cm^{-1}, which are ascribed to $^2B_{1g}(F)\rightarrow{}^2B_{1g}$ and $^2B_{1g}(F)\rightarrow{}^2B_{2g}$ respectively transitions suggesting octahedral geometry, and this is emphasized by its magnetic moment value of 1.76 BM [25, 26]. The $[Co(HTDP)_2]$ exhibited two transition at 24,390 and 18,518 cm^{-1} which are to $^4T_{1g}(F)\rightarrow{}^4T_{2g}(P)$ (ν2) and $^4T_{1g}(F)\rightarrow{}^4T_{2g}(F)$ (ν1) respectively. The magnetic moment value of 4.3BM and transitions are represented as octahedral geometry [25-30]. Similarly, in the case of $[Ni(HTDP)_2]2H_2O$ a transition at 22,573 cm^{-1} is assigned to the $^3A_{2g}(F)\rightarrow{}^3T_{1g}(F)$ and another transition at 19,120 cm^{-1} is assigned to $A_{2g}(F)\rightarrow{}^3T_{1g}(F)$ [31, 32]. The observed electronic transitions and the magnetic moment value of 3.2BM suggest an octahedral geometry for the complex. The electronic transition data is represented in Table 3, and the transition shows in Supplementary Figure S2.

Table 3. Electronic spectral data for ligand and its complexes.

Compounds	Absorptions in cm^{-1}	Transitions assignment	Geometry μ_{eff}(BM)
HTDP	24,691	n→π *	
$[Cu(HTDP)_2]H_2O$	24,570 18518	$^2B_{1g}(F)\rightarrow{}^2B_{1g}$ $^2B_{1g}(F)\rightarrow{}^2B_{2g}$	1.76BM
$[Co(HTDP)_2]$	24,390 18,518	$^4T_{1g}\rightarrow{}^4T_{2g}(P)$ $^4T_{1g}\rightarrow{}^4T_{2g}(F)$	4.3BM
$[Ni(HTDP)_2]2H_2O$	22,573 19,120	$^3A_{2g}(F)\rightarrow{}^3T_{1g}(F)$ $A_{2g}(F)\rightarrow{}^3T_{1g}(F)$	3.2BM

3.5. Mass spectral studies.

The molecular ion peak of HTDP appeared at m/z 449 (M+1). The value matches the expected mass. The molecular peak (M+1) observed in the mass spectra of $[Cu(HTDP)_2]H_2O$, $[Co(HTDP)_2]$, and $[Ni(HTDP)_2]2H_2O$ are at 977.5, 954.5, and 990.3 respectively as shown in Figure 2.

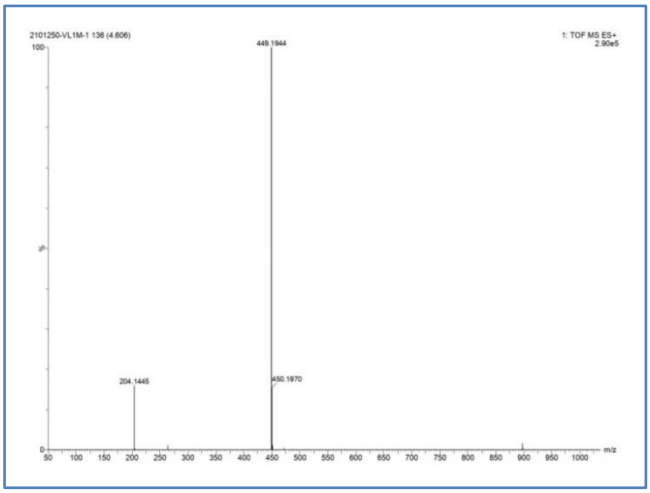

Figure 2. Mass spectrum of HTDP.

3.6. Powder XRD spectral studies.

The synthesized $[Cu(HTDP)_2]H_2O$, $[Co(HTDP)_2]$, and $[Ni(HTDP)_2]2H_2O$ complexes were studied, and the degree of crystallinity was determined from the powder X-ray diffraction patterns. The powder X-ray diffraction pattern of $[Cu(HTDP)_2]H_2O$ showed 6 reflections in the range of 9-30°. The $[Co(HTDP)_2]$ showed 5 peaks in the region 9.2-27°, and 9 peaks

appeared for $[Ni(HTDP)_2]2H_2O$ in the range at 6-28°, and their spectra are represented in Figure 3. The inter-planer spacing (d) has been calculated from the positions of intense peaks (2θ) using Bragg's equation $n\lambda=2d\sin\theta$ (where λ= 1.5406 Å). Further, the unit cell parameter was calculated for cubic symmetry from the obtained peaks, and $h^2 + k^2 + l^2$ values were determined and tabulated in Table 4. The calculated lattice parameter a=b=c of $[Cu(HTDP)_2]H_2O$ is 9.35, $[Co(HTDP)_2]$ is 9.28, while for $[Ni(HTDP)_2]2H_2O$ is found to be 13.2. The presence of forbidden numbers 7 and 15 in the observed results indicates that the $[Ni(HTDP)_2]2H_2O$ complex may belong to hexagonal or tetragonal systems [28-34].

Table 4. XRD spectral data.

Compound	Point	2θ	Sinθ	$Sin^2\theta$	$Sin^2\theta\times1000$	$h^2+k^2+l^2$	h k l	D		a in Å
								Obs	Cal	
$[Cu(HTDP)_2]H_2O$	1	9.21	0.080	0.0064	6.4	1(1)	1 0 0	9.5	9.5	9.6
	2	9.5	0.082	0.0067	6.7	1.04(1)	1 0 0	9.2	9.2	9.5
	3	14.8	0.128	0.0160	16	2.5(3)	1 1 1	5.9	5.5	9.6
	4	19.3	0.167	0.0270	27	4.21(4)	2 0 0	4.5	4.9	9.9
	5	23.12	0.199	0.0390	39	6.09(6)	2 1 1	3.7	3.8	9.4
	6	26.1	0.220	0.0480	48	7.5(8)	2 2 0	3.4	3.2	9.6
$[Co(HTDP)_2]$	1	9.28	0.080	0.0064	6.4	1(1)	1 0 0	9.5	9.4	9.4
	2	14.86	0.120	0.0144	14.4	2.11(2)	1 1 0	6.1	6.5	9.1
	3	17.2	0.140	0.0190	19	2.91(3)	1 1 1	5.1	5.4	9.3
	4	19.4	0.165	0.0272	27.2	4.27(4)	2 0 0	4.5	4.7	9.4
	5	26.5	0.228	0.0519	51.9	8.10(8)	2 2 0	3.3	3.2	9.2
$[Ni(HTDP)_2]2H_2O$	1	6.4	0.060	0.0036	3.6	1(1)	1 0 0	13	12.9	13
	2	9.2	0.080	0.0064	6.4	1.77(2)	1 1 0	9.2	9.5	13.7
	3	10.2	0.088	0.0077	7.7	2.13(2)	1 1 0	8.9	8.5	13
	4	14.8	0.128	0.0163	16.3	4.58(5)	2 1 0	5.9	5.9	13.6
	5	16.12	0.139	0.0193	19.3	5.3(5)	2 1 0	5.8	5.4	13
	6	17.2	0.149	0.0222	22.2	6.1(6)	2 1 1	5.4	5.2	13.3
	7	18.3	0.159	0.0252	25.2	7(7)	-	4.9	4.8	13.1
	8	19.4	0.168	0.0282	28.2	7.8(8)	2 2 0	4.6	4.5	13.1
	9	26.6	0.230	0.0529	52.9	14.6(15)	-	3.3	3.3	13

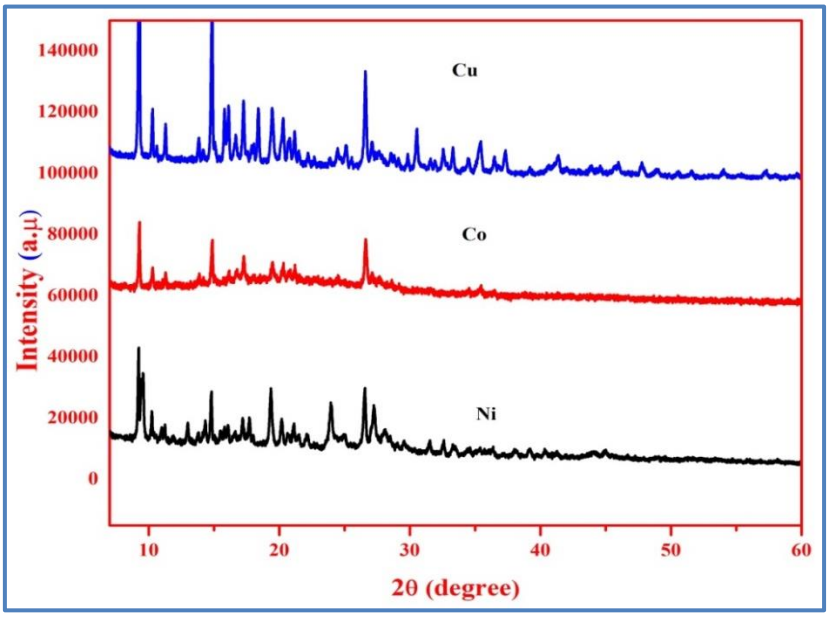

Figure 3. Powder XRD patterns of Cu, Co, and Ni complexes.

3.7. Thermal analysis of the compound.

The thermal analysis of $[Cu(HTDP)_2]H_2O$, $[Co(HTDP)_2]$ and $[Ni(HTDP)_2]2H_2O$ were carried out to understand the thermal stability and the weight loss of the complexes from the laboratory temperature to 1000 °C at a heating rate of 10 °C/min an N_2 atmosphere. The

temperatures versus weight loss percentage are plotted and shown in Figure 4. The $[Cu(HTDP)_2]H_2O$ indicates three degradation steps. In the first step, a weight loss of 8.14 % occurred in the region 43-177°C due to the loss of one H_2O and $4CH_3$ [35]. In the second stage, the weight loss of 35.8% appeared in the temperature range 177-476 °C corresponding to loss of $C_{14}H_{10}N_6S_2O$ moiety, and in the third stage, 50 % weight loss occurred from 476-667°C due to the dissociation of $C_{26}H_{20}N_6O_4$ moiety. Finally, CuO remains.

In the case of $[Co(HTDP)_2]$, the weight loss that occurred initially, amounting to 20.9 %, has appeared at 65-286 °C due to the dissociation of $C_6N_4S_2$. The second stage of weight loss, 36.5 %, occurred in the temperature region 286-481°C because of the dissociation of $C_{17}H_{16}N_4O_4$ moiety. The third stage attributed to eliminating 36.2 % of $C_{21}H_{21}N_4O$ moiety in the range 481-594 °C, leaving behind CoO as residue [36].

In the $[Ni(HTDP)_2]2H_2O$, a weight loss in the region 42-179 °C of about 9.4 % corresponds to two lattice water molecules. In the second stage, 42.2 % weight loss due to the loss of $C_{20}H_{14}N_6S_2O$ in the region at 179-476 °C. Further, the third stage of weight loss from 476 to 601 °C due to 41 % of $C_{20}H_{15}N_6O_4$ moiety. Finally, NiO residue remained [37, 38]. The weight loss data are given in Table 5, and degradation curves are shown in Figure 4.

Table 5. Thermal degradation.

Complex	Step	Decomposition Temp °C	Assignment	Loss of mass in (%)	Residue species
$[Cu(HTDP)_2]H_2O$	1	43-177	H_2O & $4CH_3$	8.14 %	CuO
	2	177-476	$C_{14}H_{10}N_6S_2O$	35.8%	
	3	476-667	$C_{26}H_{20}N_6O_4$	50.1%	
$[Co(HTDP)_2]$	1	65-286	$C_6N_4S_2$	20.9%	CoO
	2	286-481	$C_{17}H_{16}N_4O_4$	36.5%	
	3	481-594	$C_{21}H_{21}N_4O$	36.2%	
$[Ni(HTDP)_2]2H_2O$	1	42-179	$2H_2O$ & $4CH_3$	9.5%	NiO
	2	179-476	$C_{20}H_{14}N_6S_2O$	42.2%	
	3	476-601	$C_{20}H_{15}N_6O_4$	41 %	

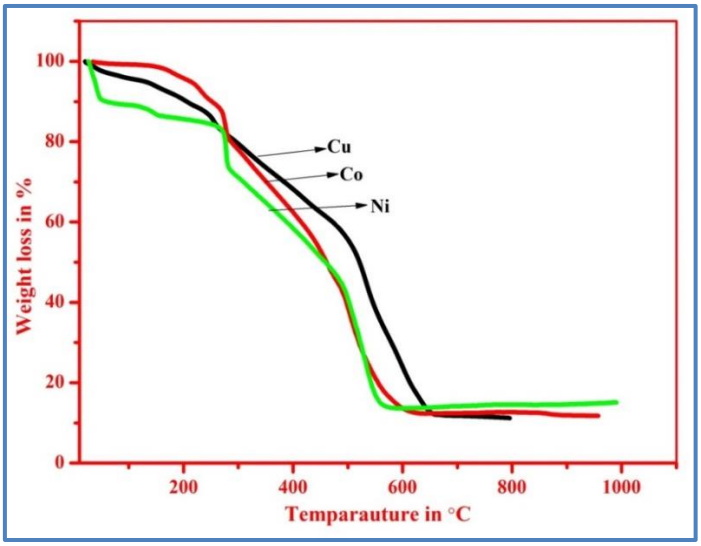

Figure 4. TGA curves for $[Cu(HTDP)_2]H_2O$, $[Co(HTDP)_2]$ and $[Ni(HTDP)_2]2H_2O$.

3.8. Electrochemical methods.

3.8.1. Charge transfer behavior of modified electrode.

The charge transfer behavior of $[Co(HTDP)_2]$ modified sensor was investigated using $K_4[Fe(CN)_6]$, which behaves as a redox system. The bare glassy carbon electrode (GCE)

displayed Ferri/ferrocyanide system in CV response. The electrochemical evaluation in 0.5 mM $K_4[Fe(CN)_6]$ solution at a scan rate of 50 mVs^{-1} between bare GCE and modified $[Co(HTDP)_2]$/GC electrodes is represented in Figure 5. The modified GCE exhibited more current response in the redox system because the cobalt complex has good electro-conducting properties compared to bare GCE. The electrode acts as a bridge of electron transfer between electrode surface (GCE) and buffer solution in cyclic voltmeter [15, 39].

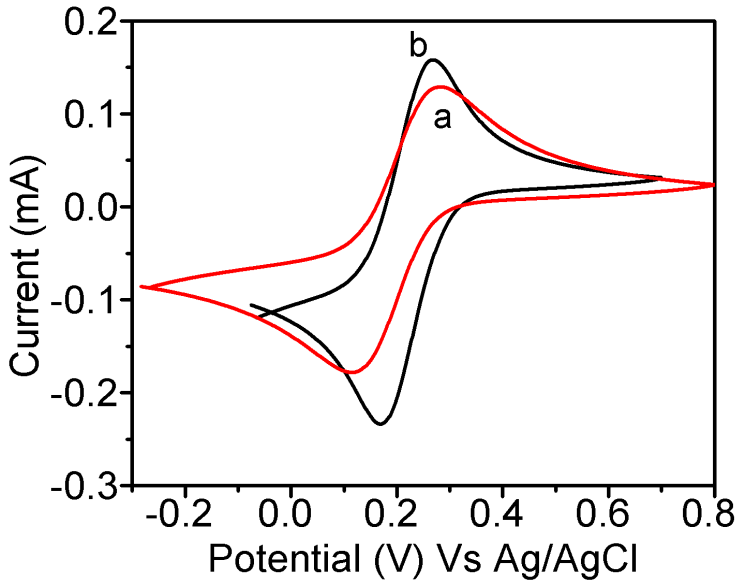

Figure 5. Cyclic voltammogram of 0.5M KCl solution containing 5 mM $K_3[Fe(CN)_6]$/ $K_4[Fe(CN)_6]$ at the **a)** bare GCE and **b)** $[Co(HTDP)_2]$/GCE, the scan rate:50 mVs^{-1}.

3.8.2. Electrochemical investigation of the different electrodes.

Electrochemical sensing of nitrate was studied in an electrolytic solution using a phosphate buffer solution of pH 7. The cyclic voltammogram of (i) bare GCE, (ii) $[Co(HTDP)_2]$/GCE , and (iii) $[Co(HTDP)_2]$/GCE with 02 µL concentration of $NaNO_2$ at a scan rate of 50 mVs^{-1}. The modified $[Co(HTDP)_2]$/GC electrode showed intensified peak current responses as compared to the bare glassy carbon electrode, and it is a good electrochemically active, as represented in Figure 6 [16, 39].

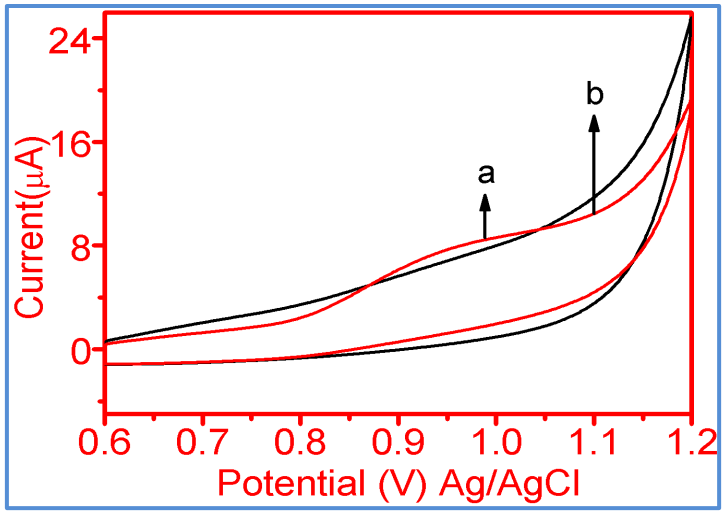

Figure 6. Cyclic voltammogram of different electrodes **(a)** Bare GCE and **(b)** Modified electrode in PBS pH 7 with the scan rate of 50 mVs^{-1}.

3.8.3. Electrochemical determination of nitrate.

Electrochemical detection of nitrate using modified [Co(HTDP)$_2$]/GC electrode by CV technique. In the modified electrode in PBS pH 7.0, the CV curves showed an increase in peak current response compared to bare GCE. While adding the various concentrations of nitrate, the peak current increases gradually with a slight shift in the potential towards the negative side; therefore, the modified electrode can detect the nitrate with a long linear range, lower sensitivity, and LOD. The linear range of (10 to 80 μmolL^{-1}), sensitivity is (0.172 μAμM^{-1}cm$^{-2.}$), and LOD is 3.333 μML^{-1}. Thus, the modified electrode exhibits highly electroactive properties, as shown in Figure 7 [15, 39].

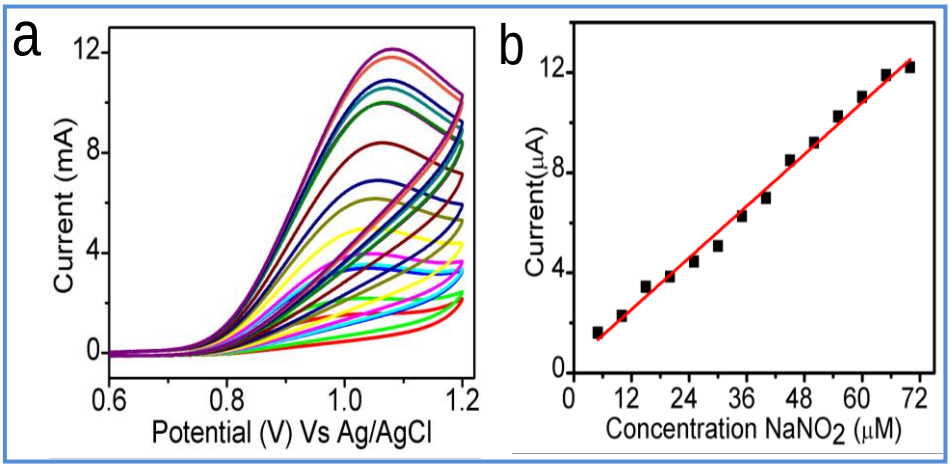

Figure 7. (a) Cyclic voltammogram of nitrite at [Co(HTDP)$_2$]/GCE concentration ranging from (10–80 μM); **(b)** Inset: Calibration plot of current vs. concentration of $NaNO_2$.

3.8.4. Effect of scan rate.

The modified GCE while subjected to a pH 7 buffer solution containing 10 μM of nitrate under various scan rates from 10 to 150 mVs^{-1}. As the scan rate increases, the peak current increases linearly as calculated by the linear regression equation, Ipa (μA) = 0.918 (μM) + 0.0609 and R^2 = 0.9959. These analytical results confirm [Co(HTDP)$_2$] that the modified electrode was a surface adsorbed process, as shown in Figure 8 [40].

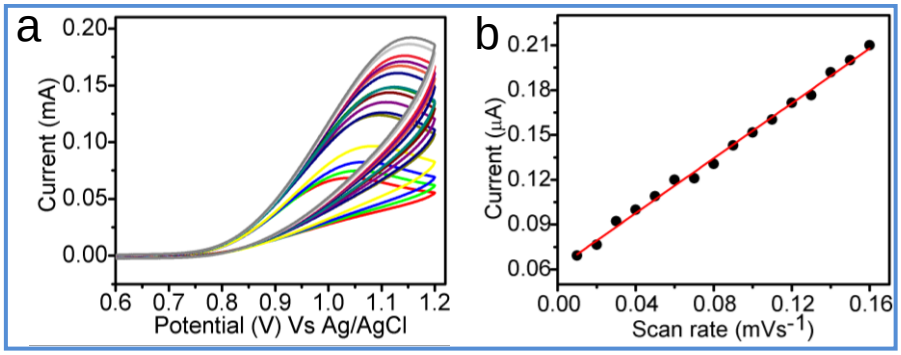

Figure 8. (a) Cyclic voltammogram of nitrite at [Co(HTDP)$_2$] modified GCE scan rate ranging from (10 - 150mVs^{-1}). **(b)** Inset plot of current (I) vs. Scan rate.

3.8.5. Differential pulse voltammetry (DPV) studies of nitrate.

DPV was one of the best techniques for detecting $NaNO_2$ using modified [Co(HTDP)$_2$]/GCE, and it gives accurate results for the detection of nitrate; it was conducted in PBS pH 7, and the results are collected in Table 6. The reaction which occurs, as mentioned

below, showed enhanced anodic peak current response compared to bare GCE. The increasing concentration of $NaNO_2$ in the range from 0.1 to 01 $\mu molL^{-1}$ and the peak current enhanced at the fixed potential. The analytical profile of the modified electrode was long linear range 0.1-01 $\mu molL^{-1,}$ sensitivity 11.043 $\mu A\mu M^{-1}cm^{-2}$ and LOD is 0.0333μML^{-1}. Further, the modified sensor shows reproducible and anti-leaching properties, as shown in Figure 9; the electrochemical behavior of the electron is shown in the below equations [41].

$$2[Co(II)(HTDP)_2] \longrightarrow 2[Co(III)(HTDP)_2]$$
$$2[Co(III)(HTDP)_2] + 2NO_2^- \rightleftharpoons 2[Co(II)(HTDP)_2 + NO_2]$$
$$2[Co(II)(HTDP)_2 + NO_2 \not\longrightarrow 2[Co(III)(HTDP)_2] + 2NO_2^- + 2e^-$$
$$2NO_2 + H_2O \rightleftharpoons 2H^+ + NO_3^- + NO_2^-$$

Table 6. Comparison of the different actuators for nitrite determination.

Compound	Linear range $\mu molL^{-1}$	Technique	LOD μML^{-1}	Sensitivity ($\mu A\ \mu M^{-1}\ cm^{-2}$)	Reference
CoTM-QOPc /CNP/GCE	0.2-200 0.2-225	CV DPV	0.06 0.06	2.298 1.031	15
CoL/MNSs/CPE	0.2-30.0	SWV	0.015	-	39
Co_3O_4/RGO	1-380	CV	0.14	29.5	40
CRS/BN-RGO/GCE	0.001- 1290	DPV	0.0159	1.5309	41
$[Co(HTDP)_2]$/GCE	10-80 0.1-1	CV DPV	3.333 0.0333	0.172 11.043	**This work**

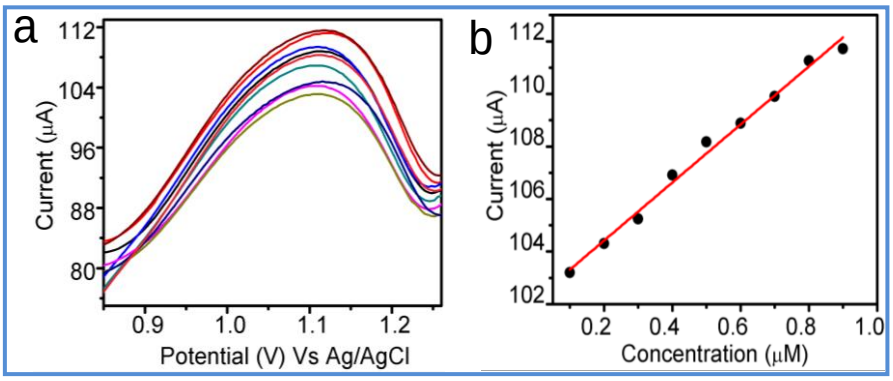

Figure 9. (a) DPV of $[Co(HTDP)_2]$/GCE at a concentration ranging from 0.1– 10 µM/L. (**b**) Inset: Calibration graph of current vs. concentration.

3.8.6. Real samples analysis.

The experimental feasibility of the $[Co(HTDP)_2]$/GCE was applied to examine the nitrite range in different milk sources using a standard addition method. The results were noted in Table 7. Initially, each individual milk source was filtered with 0.1 M of pH 7 PBS as described in the Chinese National Food Safety Standard [42] and appeared in 92–103% range. These results reveal the experimental feasibility of the drop-coated electrode for analysis of nitrite in real samples.

Table 7. Determination of nitrite in milk samples.

Sample	Added ($\mu molL^{-1}$)	Detected ($\mu molL^{-1}$)	Recovery (%)
Milk 1	5	4.60	92
	10	10.06	100.6
	15	14.84	98.93
Milk 2	5	4.45	89
	10	10.33	103.3
	15	14.94	99.6

3.9. Biological studies.

3.9.1. Antimicrobial activities.

The HTDP and their synthesized metal complexes were tested for antimicrobial cultures by agar well diffusion technique using Nystatin and Chloramphenicol as standard drugs. The zone of inhibition area in activities was measured by millimeters (mm) and was repeated three times to assess the effectiveness of the antimicrobial activity. Ligand showed a good positive result, and its complexes showed enhanced growth inhibition against an antimicrobial activity as compared to the uncoordinated ligand. Because metals were bonded with donating atoms of the ligand having delocalized electrons in the chelating rings system, the lipophilic property increases [43, 44]. The result was explained through Tweedy's chelation theory and Overtone's theory [45-47]. Moreover, the $[Cu(HTDP)_2]H_2O$ and $[Co(HTDP)_2]$ showed the best result with *S.aureus*, *E.coli*, and *fusarium* microbial cultures. The values are recorded in Tables (8 and 9), and the results are represented in Figures 10 to 12.

Figure 10. Antibacterial zone of inhibition by HTDP and its metal complexes**.**

Table 8. Antibacterial activity of the HTDP and its metal complexes.

Bacterial cultures	Cont. in mg/ml	Growth inhibition in mm				
		HTDP	$[Cu(HTDP)_2]H_2O$	$[Co(HTDP)_2]$	$[Ni(HTDP)_2]2H_2O$	STD
S.aureus	0.25	2.03 ± 0.05	8.03 ± 0.05	6.03 ± 0.05	2.03 ± 0.05	16 ± 0
	0.5	2.2 ± 0.2	9.03 ± 0.05	10.03± 0.05	8.03 ± 0.05	16 ± 0
	0.75	2.3 ± 0.35	09.2 ± 0.25	11.06 ± 0.1	8.3 ± 0.6	16 ± 0
	1	2.4 ± 0.3	10.03 ± 0.05	14 ± 0	9.03 ± 0.05	16 ± 0
Clostridium	0.25	3 ± 0	8.03 ± 0.05	7.03 ± 0.05	5.03 ± 0.05	16 ± 0
	0.5	4.06 ± 0.1	10.03 ± 0.05	12.03 ±0.05	8.03 ± 0.05	16 ± 0
	0.75	4.13 0.15	10.16 ± 0.28	11.16 ±0.28	8.8 ± 0.07	16 ± 0
	1	4.2 ± 0.25	12.06 ± 0.11	13.03 ±0.05	9.03 ± 0.05	16 ± 0
E. coli	0.25	3.1 ± 0.1	9.03 ± 0.05	5.03 ± 0.05	5.03 ± 0.05	18 ± 0
	0.5	4.1 ± 0.1	9.3 ± 0.05	11.03 ±0.05	7.03 ± 0.05	18 ± 0
	0.75	4.2 ± 0.15	12.03 ± 0.05	13.03 ±0.05	9.03 ± 0.05	18 ± 0
	1	4.2 ± 0.15	12.03 ± 0.05	13.03 ±0.05	9.03 ± 0.05	18 ± 0
Shigella	0.25	2.2 ± 0.34	8.03 ± 0.05	9.03 ± 0.05	5.1 ± 0.17	16 ± 0
	0.5	4.1 ± 0.1	8.16 ± 0.15	9.16 ± 0.28	8.06 ± 0.1	16 ± 0
	0.75	4.13 ± 0.1	9.16 ± 0.15	11.26 ± 0.4	9.1 ± 0.3	16 ± 0
	1	4.16± 0.15	10.03 ± 0.05	12.03 ±0.05	9.16 ± 0.2	16 ± 0

*Each value is displayed average ± SD (standard division) of three replicates for the zone of inhibition.
*STD: Chloramphenicol.

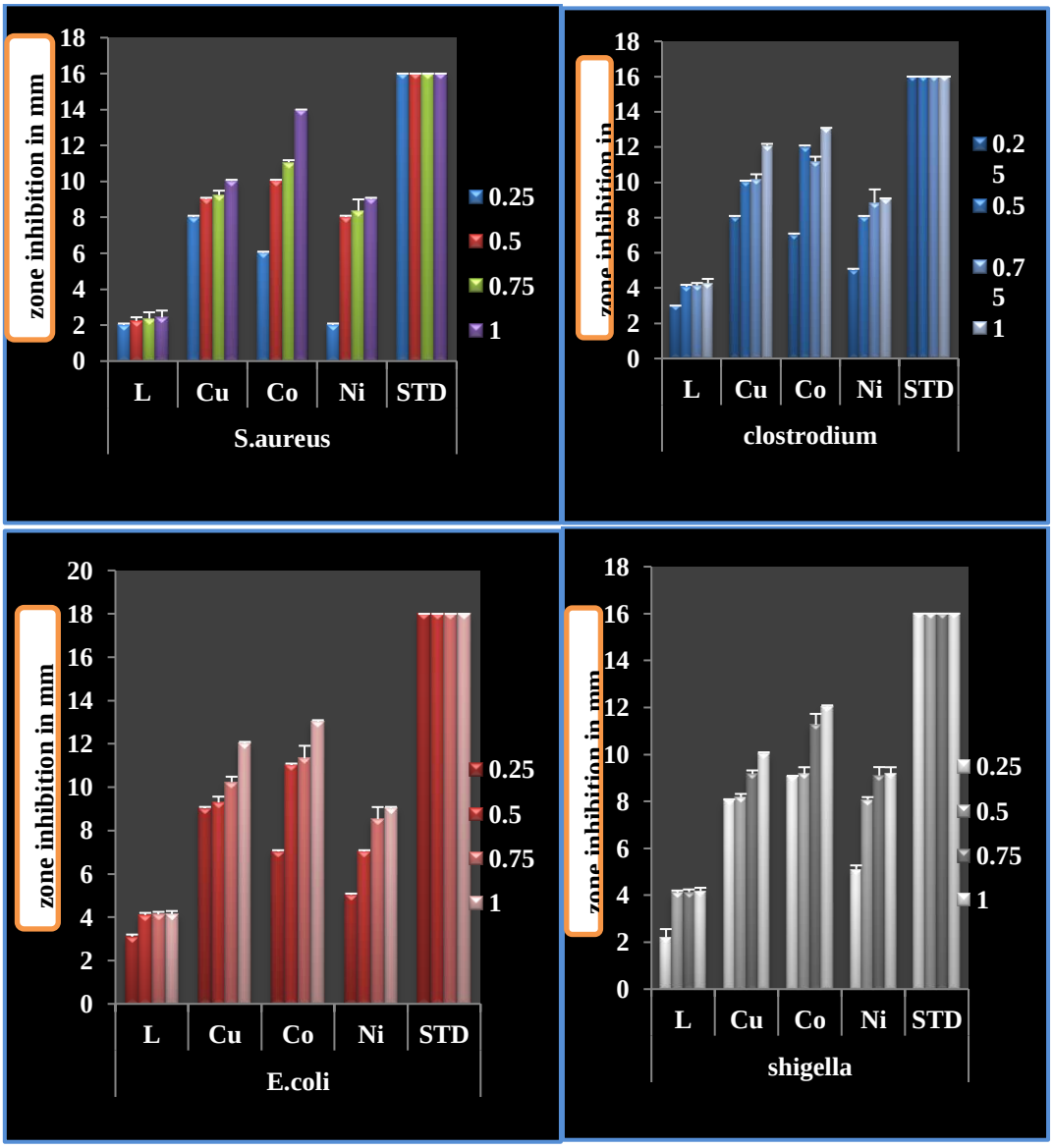

Figure 11. Graphical representation of antibacterial zone of inhibition activity of HTDP and its metal complexes.

Table 9. Antifungal activity of HTDP and its metal complexes.

Fungal cultures	Cont. in mg/ml	Growth inhibition in mm				
		HTDP	$[Cu(HTDP)_2]H_2O$	$[Co(HTDP)_2]$	$[Ni(HTDP)_2]2H_2O$	STD
Aspergillus	0.25	1 ± 0	4.03 ± 0.05	6.03± 0.05	3.03± 0.05	12 ± 0
	0.5	1.13 ± 0.05	6.2 ± 0.26	8.06 ± 0.11	5.03 ± 0.05	12 ± 0
	0.75	2.03 ± 0.05	8.03 ± 0.05	10.03 ± 0.07	6.06 ± 0.11	12 ± 0
	1	2.2 ± 0.26	8.33 ± 0.2	10.1 ± 0.17	8.03 ± 0.05	16 ± 0
Fusarium	0.25	1.03 ± 0.05	5.03 ± 0.05	7.05 ± 0.05	2.03 ± 0.05	10 ± 0
	0.5	1.03 ± 0.05	5.03 ± 0.05	7.05 ± 0.05	2.03 ± 0.05	10 ± 0
	0.75	1.23 ± 0.25	8.06 ± 0.11	11.06 ± 0.11	6.1 ± 0.17	10 ± 0
	1	4 ± 0	9.03 ± 0.05	12.03 ± 0.05	10.03 ± 0.05	12 ± 0

*Each value is displayed average ± SD (standard division) of three replicates for the zone of inhibition.

*STD: Nystatin

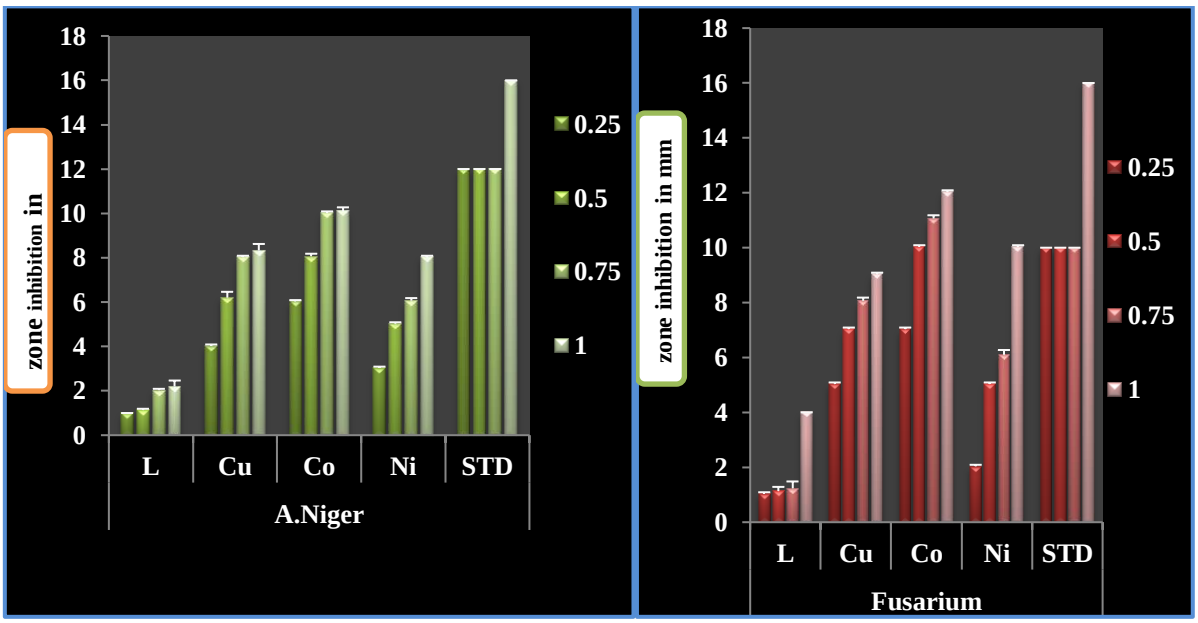

Figure 12. Graphical representation of the antifungal activity of HTDP and its metal complexes.

3.9.2. Antidiabitic studies.

The synthesized HTDP and its metal complexes screened for antidiabetic activity. Inhibitions of enzymes manage the stage of insulin and glucose level in blood over a long period and also control the risk of hyperglycemia. Inhibition screening was recorded with various concentrations of 25, 50, and 100 µg/mL shown in Figure 13. Further, HTDP exhibited 10.2, 24.03, and 33.23% inhibition activity, and its complexes showed enhanced inhibitory percentage results [48].

Table 10. Antidiabetic activity of the ligand and their metal complexes.

Cont. in µg/mL	Alpha amylase inhibitory activity in %				
	HTDP	$[Cu(HTDP)_2]H_2O$	$[Co(HTDP)_2]$	$[Ni(HTDP)_2]2H_2O$	STD
25	10.2±0.25	22.5±0.43	35.16±1.6	34.06±0.11	36.66±2.08
50	24.03±0.05	29±0	45.2±0.34	46.3±0.51	49.66±3.05
1	33.23±0.40	57±0.6	84.03±0.57	78.76±0.58	92.6± 0.6

*STD Acarbose (Acb) is the standard of alpha-amylase enzyme activity, M ± SD.

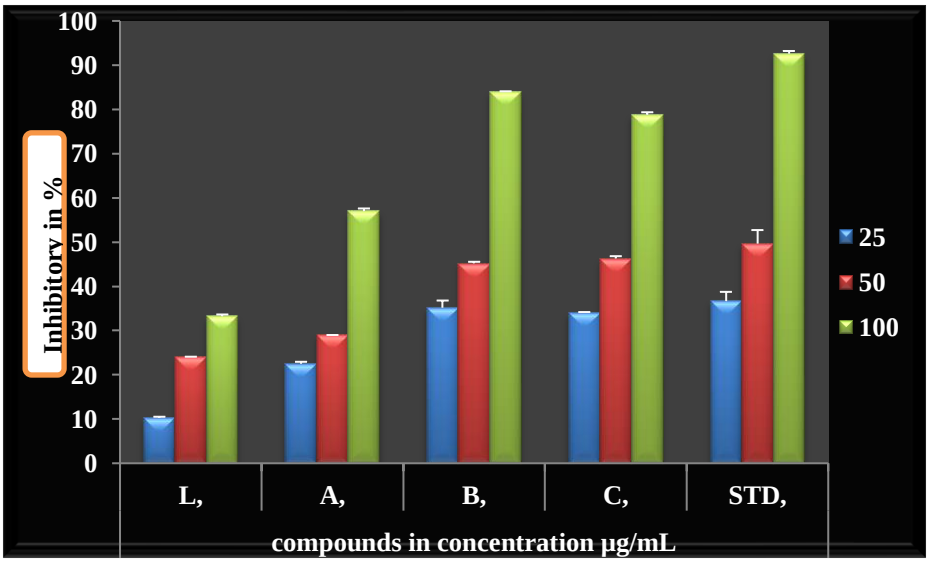

Figure 13. Graph representation of antidiabetic activities of ligand and its metal complexes.

Among the synthesized complexes, the $[Co(HTDP)_2]$ showed higher inhibitory growth, as shown in Table 10. The potency of the synthesized compound was measured by the IC_{50} method. It indicates how much drug is needed to inhibit a biological process by half. The IC_{50} of HTDP showed at 153.50 µg/mL, and its $[Cu(HTDP)_2]H_2O$ showed 87.28 µg/mL, $[Co(HTDP)_2]$ exhibited 51.16 µg/mL while $[Ni(HTDP)_2]2H_2O$ showed IC_{50} of 47.08 µg/mL, standard acarbose drug which was found to have 45.68 µg/mL as shown in figure 14 [48-52]. The data is given in table 11.

Table 11. IC_{50} value of ligands and their metal complexes against an alpha-amylase antidiabetic agent in µg/mL.

Compounds	IC_{50} value in µg/mL	R^2
HTDP	153.50±0.26	0.915
$[Cu(HTDP)_2]H_2O$	87.29±0.51	0.971
$[Co(HTDP)_2]$	51.16±0.58	0.985
$[Ni(HTDP)_2]2H_2O$	47.08±0.05	0.991
Acb	45.68±0.39	0.988

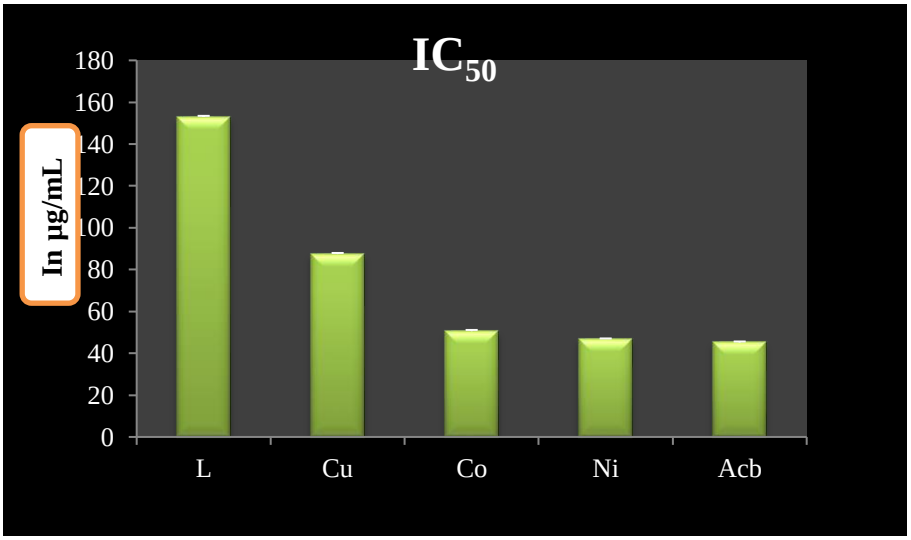

Figure 14. Graph representation of IC_{50} of ligand and its metal complexes in µg/mL against alpha-amylase enzyme activity.

3.9.3. Anti-mycobacterium studies.

Synthesized HTDP and its metal complexes were screened for Mycobacterium tuberculosis strain using tetrazolium salt indicator (MTT) for anti-mycobacterial (M-TB) activity it spread in the eukaryotic area. The color change in the well revealed inhibition of bacterial growth. The MIC percentages were recorded at 37 °C incubation in different concentrations of 25, 50, and 100 µg/mL with organic anti-infective bacterium drug agent Chloramphenicol (CHL) as standard. The HTDP showed 12, 15, and 22 % activity, and its metal complexes exhibited enhanced inhibition because HTDP act as a charge transfer to the central metal atom. Thus, the complexes form a good binding; therefore, They are stable bioactive molecules. Moreover, the $[Co(HTDP)_2]$ and $[Ni(HTDP)_2]2H_2O$ showed better percentage inhibition at 50 µg/mL, as shown in Figure 15. The MIC was evaluated by three replicate measurements, as shown in Table 12, and its mean inhibition values find the dose efficiency of compounds as calculated by Y=MX+C, IC50(X) =Y-C/M. The HTDP IC_{50} has 317.04 µg/mL, and their $[Cu(HTDP)_2]H_2O$, $[Co(HTDP)_2]$, and $[Ni(HTDP)_2]2H_2O$ had better half-maximum inhibitory concentration values as tabulated in table13 and the graph showed in figure16 [53].

Table 12. Anti-tuberculosis zone inhibition of ligands and their metal complexes against M. Tuberculosis.

Cont. in µg/mL	Mycobacterial tuberculosis activity in %				
	HTDP	$[Cu(HTDP)_2]H_2O$	$[Co(HTDP)_2]$	$[Ni(HTDP)_2]2H_2O$	CHL
25	12±0.25	22.5±0.43	39.16±1.6	43.06±0.11	13.66±2.08
50	15.03±0.05	35±0	52.2±0.34	54.3±0.51	30.66±3.05
100	22.23±0.40	57±0.6	81.03±0.57	60.76±0.58	72.6± 0.6

*Chloramphenicol (CHL) is considered a standard antibiotic drug. M ± SD.

Table 13. IC_{50} value of ligand and their metal complexes against anti-mycobacterium tuberculosis agent in µg/mL.

Compounds	IC_{50} value in µg/mL	R^2
HTDP	317.04 ±0.05	0.997
$[Cu(HTDP)_2]H_2O$	84.14 ± 0.165	0.996
$[Co(HTDP)_2]$	45.17 ± 0.156	0.998
$[Ni(HTDP)_2]2H_2O$	48.17 ± 0.282	0.904
CHL	73.04 ±0.05	0.997

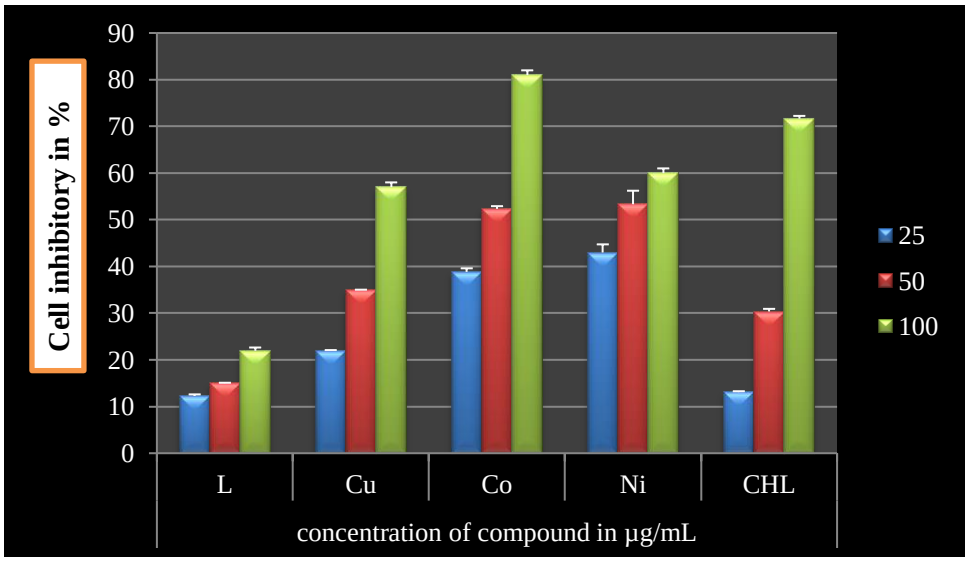

Figure 15. Graphical representation of anti-tuberculosis activities of ligand and its metal complexes.

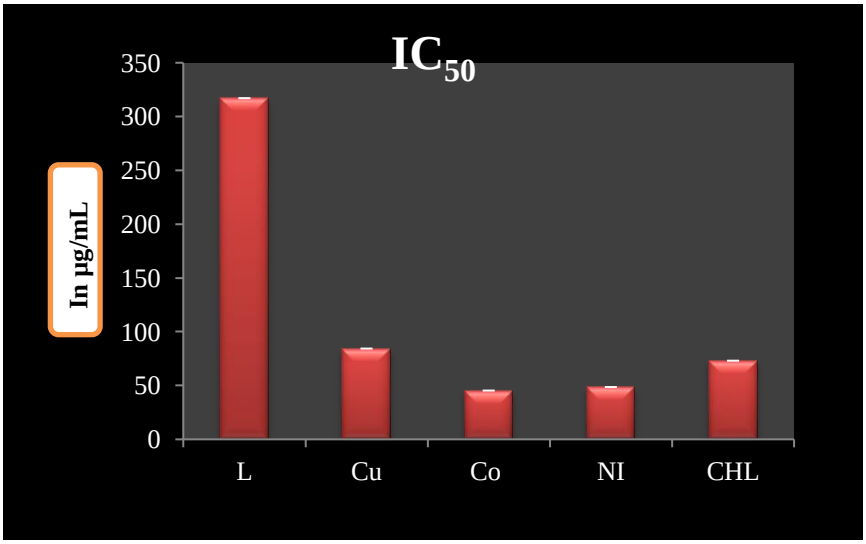

Figure 16. Graph represented IC_{50} values of ligand and its metal complexes in µg/mL against for mycobacterium agent.

4. Conclusions

In this present investigation, novel HTDP and its coordinated Cu(II), Co(II), and Ni(II) complexes have been synthesized and characterized by various analytical techniques. The molar conductance values indicate the non-electrolytic nature of complexes. Based on UV–Vis

and magnetic susceptibility data, the synthesized complexes proposed to have octahedral geometry. The thermal analysis data showed the mode of degradation of the metal complexes. The modified $[Co(HTDP)_2]$/GCE showed highly electroactive with nitrate sensing is 0.172 µA $\mu M^{-1}cm^{-2}$ by the cyclic voltammeter, and the differential pulse voltammeter showed 11.043 µA μM^{-1} cm^{-2}. The uncoordinated HTDP and their complexes were screened for antimicrobial culture. The clostridium E. coli and fusarium showed better growth of zone inhibition and $[Cu(HTDP)_2]H_2O$ and $[Co(HTDP)_2]$ exhibiting promising results. Inhibition of α-amylase showed positive activity with a potential IC_{50} value for $[Ni(HTDP)_2]2H_2O$ with 47.08 % inhibition activity, and it is best for diabetic patience and known as starch blockers because they assist dietary of glucose in the antidiabetic study. The $[Co(HTDP)_2]$ and $[Ni(HTDP)_2]2H_2O$ complexes showed good drug potency when compared to the uncoordinated ligand. The HTDP and its complexes showed enhanced activity and can be used as a potent agent against selective pathogens.

Funding

This research received no funding.

Acknowledgments

The authors thank the Manipal Institute of Technology, SAIF Dharwad, SJM College of Pharmacy, Chitradurga, and the University of Mysore for providing spectral facilities. The authors also thank Biotech Pvt Mysore, Karnataka, India, for biological studies.

Conflicts of Interest

The research authors declared no conflict of interest.

References

1. Venugopal, N.; Krishnamurthy, G.; Bhojya Naik, H.S.; Manohara, J.D. DNA Binding, Molecular Docking and Antimicrobial Evaluation of Novel Azo Dye Ligand and Their Metal Complexes. *Journal of Inorganic and Organometallic Polymers Materials* **2019,** *30*, 2608-2625, https://doi.org/10.1007/s10904-019-01394-8.
2. Saad, F.A.; El-Ghamry, H.A.; Kassem, M.A. Synthesis, structural characterizationand DNA binding affinity of new bioactive nano-sized transitionmetal complexes with sulfathiazole azo dye for therapeutic applications. *Appl Organometal Chem* **2019,** *33*, 4965, https://doi.org/10.1002/aoc.4965.
3. Mohamed, Gaber.; Fathalla, S.K.; El-Ghamry, H.A. 2,4-Dihydroxy-5-[(5-mercapto-1H-1,2,4-triazole-3-yl)diazenyl] benzaldehyde acetato, chloro and nitrato Cu(II) complexes: Synthesis, structural characterization, DNA binding and anticancer and antimicrobial activity. *Appl Organometal Chem* **2019,** *33*, 4707, https://doi.org/10.1002/aoc.4707.
4. Kirthan, B.R.; Prabhakara, M.C.; Bhojya naik, H.S.; Viswanath, R.; Amith Nayak, P.H. Optoelectronic, photocatalytic and biological studies of mixed ligand Cd(II) complex and its fabricated CdO nanoparticles. *Journal of Molecular Structure* **2021,** *1244*, 130917, https://doi.org/10.1016/j.molstruc.2021.130917.
5. Alotaibi, S.H.; Radwan, A.S.; Abdel-Monem, Y.K.; Makhlouf, M.M. Synthesis, thermal behavior and optical characterizations of thin films of a novel thiazole azo dye and its copper complexes. *Molecular and Biomolecular Spectroscopy* **2018,** *205*, 364–375, https://doi.org/10.1016/j.saa.2018.07.043.
6. Ranjitha, N.; Krishnamurthy, G.; Bhojya Naik, H.S.; Malathesh, Pari.; Lubna, Afroza.; Sumadevi, K.R.; Manjunatha, M.N. Structural elucidation, Voltammetric detection of dopamine, molecular docking and biological inspection of novel 4-aminoantipyrine derived Schiff bases in Co(II), Ni(II) and Cu(II) complexes. *Inorganica Chemica Acta* **2022,** *543*, 121191, https://doi.org/10.1016/j.ica.2022.121191.
7. Muhammad, Sirajuddin.; Noor-Uddin, Saqib, Ali.; Muhammad-Nawaz, Tahir. Potential bioactive Schiff base compounds: Synthesis, characterization, X-ray structures, biological screenings and interaction with Salmon

sperm DNA. *Molecular and Biomolecular Spectroscopy* **2013,** *116*, 111-121, http://dx.doi.org/10.1016/j.saa.2013.06.096.
8. Ravi, B.N.; Keshavayya, J.; Mallikarjuna, N.M.; VinodKumar.; Fiza-Noor Zahara. Synthesis, spectral characterization, anticancer and cyclic voltammetric studies of azo colorants containing thiazole structure. *Chemical Data Collections* **2021,** *33*, 100686, https://doi.org/10.1016/j.cdc.2021.100686.
9. Al-Adilee, K.J.; Abass, A.K.; Taher, M. Synthesis of some transition metalcomplexes with new heterocyclic thiazolyl azo dye and their uses as sensitizers in photoreactions. *Journal of Molecular Structure* **2015,** *1108*, 378-397, https://doi.org/10.1016/j.molstruc.2015.11.038.
10. Murugaiyan, Manimohan.; Sivashanmugam, Pugalmani.; Mohamed-Aboobucker, Sithique. Synthesis, Spectral Characterisation and Biological Activities of Novel Biomaterial/N, N, O Donor Tridentate Co (II), Ni (II) and Zn (II) Complexes of Hydrazide Based Biopolymer Schiff Base Ligand. *Journal of Inorganic and Organometallic Polymers and Materials* **2020,** *30*, 4481-4495, https://doi.org/10.1007/s10904-020-01578-7.
11. Xuhua, Dong.; Siqi, Xie.; Jingyang, Zhu.; Haiquan, Liu.; Yong, Zhao.; Tianjun, Ni.; Long, Wu.; Yongheng, Zhu. Mesoporous CoOx/C Nanocomposites Functionalized Electrochemical Sensor for Rapid and Continuous Detection of Nitrite. *Coatings* **2021,** *11*, 596. https://doi.org/10.3390/coatings11050596.
12. Ariel, Ndala.; Bamato, Itota.; Jessica, Chamier.; Sekhar, Ray.; Christopher, Sunday.; Mahabubur, Chowdhhury. Novel (CH_6+NH_3+)-fuctionozed and nitrogen doped Co_3O_4 thin film electrochemical sensor for nanmolar detection of nitrate in Neutral pH. *Electrochemica Acta* **2021,** *388*, 138556, https://doi.org/10.1016/j.electacta.2021.138556.
13. Venugopal, N.; Krishnamurthy, G.; Bhojya Naik, H.S.; Girdhar, M. Novel bioactive azo-azomethine based Cu (II), Co (II) and Ni(II) complexes, structural determination and biological activity. *Journal of Molecular Structure* **2019,** *1191*, 85-94, https://doi.org/10.1016/j.molstruc.2019.04.022.
14. Venugopal, N.; Krishnamurthy, G.; Bhojya Naik, H.S.; Madhukar, Naik.; Sunilkumar, N. Synthesis, characterization, and biological activity of Cu(II) and Co(II) complexes of novel N1 , N2 -bis(4-methyl quinolin-2-yl)benzene-1,2-diamine: CuO and CoO nanoparticles derived from their metal complexes for photocatalytic activity. *Inorganic and Nano-Metal Chemistry* **2021,** *51*, 1117-1126, https://doi.org/10.1080/24701556.2020.1814337.
15. Jilani, B.S.; Mounesh.; Malathesh, P.; Mruthyunjayachari, C.D.; Reddy, K.R.V. Cobalt (II) tetra methyl-quinoline oxy bridged phthalocyanine carbon nano particles modified glassy carbon electrode for sensing nitrite: A voltammetric study. *Materials Chemistry and Physics* **2019,** *239*, 121920, https://doi.org/10.1016/j.matchemphys.2019.121920.
16. Ranjitha, N.; Krishnamurthy, G.; Manjunatha, M.N.; Bhojya Naik, H.S.; Malathesh Pari.; Vasantakumarnaik, N.K.; Laxshmikantha, J.; Pradeepa, K. Electrochemical determination of glucose and H_2O_2 using Co(II), Ni(II), Cu(II) complexes of novel 2-(1,3-benzothiazole-2ylamino)-N-(5-choro-2hydroxyphenyl)acetamide: Synthesis, Structural Characterisation, antimicrobial, anticancer activity and docking studies. *Journal of Molecular Structure* **2022,** *1274*, 134483, https://doi.org/10.1016/j.molstruc.2022.134483.
17. Nastro, A.; Germano, M.P.; Angelo, V.D.; Marino, A.; Cannatelli, M.A. Extraction methods and bioautography for evaluation of medicinal plant antimicrobial activity, *Letters in Applied Microbiology* **2000,** *30*, 379-384, https://doi.org/10.1046/j.1472-765x.2000.00731.x.
18. Abou-Dobara, M. I.; El-Sonbati, A. Z.; Morgan, M. Influence of substituenteffects on spectroscopic properties and antimicrobial activity of 5-(40 –substituted phenylazo)- 2-thioxothiazolidinone derivatives. *World J Microbiol Biotechnol* **2013,** *29*, 119–126, https://doi.org/10.1007/s11274-012-1164-5.
19. Koçyiğit, U.M.; Parham, Taslimi.; Burak, Tüzün.; Hasan, Yakan.; Halit, Muğlu.; Emre, Güzel. 1,2,3-Triazole substituted phthalocyanine metal complexes as potential inhibitors for anticholinesterase and antidiabetic enzymes with molecular docking studies. *Journal of Biomolecular Structure and Dynamics* **2020,** *40*, 2022, https://doi.org/10.1080/07391102.2020.1857842.
20. Murugaiyan, Manimohan.; Sivashanmugam, Pugalmani.; Ravichandran, K.; Mohamed, Aboobucker, Sithique. Synthesis and characterisation of novel Cu(II)- anchoredbiopolymer complexes as reusable materials for the photocatalytic degradation of methylene blue. *RSC Advances* **2020,** *10*, 18259–18279, https://doi.org/10.1039/d0ra01724h.
21. Devidas, C. Pawar.; Sunil, V. Gaikwad.; Sonali, S. Kamble.; Priya, D. Gavhane.; Milind, V. Gaikwad.; Bhaskar, S. Dawane1. Design, Synthesis, Docking and Biological Study of Pyrazole-3,5- diamine Derivatives with Potent Antitubercular Activity. *Chemical Methodologies* **2022,** *6*, 677-690, https://doi.org/10.22034/CHEMM.2022.343572.1538.

22. Kok, Tong. Wong.; Hasnah, Osman.; Thaigarajan, Parumasivam.; Unang, Supratman.; Mohammad, Tasyriq. Che. Omar.; Mohamad, Nurul. Azmi. Synthesis, Characterization and Biological Evaluation of New 3,5-Disubstituted-Pyrazoline Derivatives as Potential Anti-Mycobacterium tuberculosis H37Ra Compounds *Molecules* **2021,** *26*, 2081, https://doi.org/10.3390/molecules26072081.
23. Rajesh, Kumar.; Devla, Bimal.; Kavita.; Manish, Kumar.; Divya, Mathur.; Jyotirmoy, Maity.; Sunil, K. Singh.; Thirumal, M.; Ashok, K. Synthesis and Antitubercular Activity of 4,5-Disubstituted N1 -(5'-deoxythymidin-5'-yl)-1,2,3-triazoles *Chemistryselect* **2020,** *5*, 8839-8845, https://doi.org/10.1002/slct.202001854.
24. Nuria, Andreu.; Taryn, Fletcher.; Nitya, Krishnan.; Siouxsie, Wiles.; Robertson, B.D. Rapid measurement of anti-tuberculosis drug activity in vitro and in macrophages using bioluminescence. *J Antimicrob Chemother* **2012,** *67*:404 –414, https://doi.org/10.1093/jac/dkr472.
25. Venugopal, N.; Krishnamurthy, G.; Bhojya Naik, H.S.; Murali, Krishna. P. Synthesis, spectral characterization and biological studies of Cu (II), Co (II) and Ni (II) complexes of azo dye ligand containing 4–amino antipyrine moiety. *Journal of Molecular Structure* **2019,** *1183*, 37-51, https://doi.org/10.1016/j.molstruc.2019.01.031.
26. Raman, N.; Sobha, S. Exploring the DNA binding mode of transition metal based biologically active compounds. *Molecular and Biomolecular Spectroscopy* **2012,** *85*, 223-234, https://doi.org/10.1016/j.saa.2011.09.065.
27. Saikumari, N. Synthesis and characterization of amino acid Schiff base and its copper (II) and its antimicrobial studies. *Materials Today: Proceedings* **2021,** *47*, 1777-1781, https://doi.org/10.1016/j.matpr.2021.02.607.
28. Sathyanarayana, D.N. Electronic Absorption Spectroscopy and Related Technique (University Press (India) **2001**.
29. Mallikarjuna, N.M.; Keshavayya, J.; Maliyappa, M.R.; Shoukat Ali, R.A.; Talwara, Venkatesh. 2018. Synthesis, characterization, thermal and biological evaluation of Cu (II), Co (II) and Ni (II) complexes of azo dye ligand containing sulfamethaxazole moiety. *Journal of Molecular Structure* **2018,** *1165*, 28-36, https://doi.org/10.1016/j.molstruc.2018.03.094.
30. Rafet, Kılınc.arslan.; Emin, Erdem. Synthesis and spectral characterization of some new azo dyes and their metal complexes. *Transition Metal Chemistry* **2007,** *32*, 102–106, https://doi.org/10.1007/s11243-006-0134-x.
31. El-Gammal, O.A.; Saad, D.A.; Al-Hossainy, A.F. Synthesis, spectral characterization,optical properties and X-ray structural studies of centrosymmetri N2S2 or N2S2O2 donor Schiff base ligand and its binuclear transition metal complexes. *Journal of Molecular Structure* **2021,** *1124*, 130974, https://doi.org/10.1016/j.molstruc.2021.130974.
32. Athulya, Das.; Anjana, Rajeev.; Sarmistha, Bhunia.; Manivel, Arunkumar.; Nithya, Chari.; Muniyandi, Sankaralingam. Synthesis, characterization an antimicrobial activity of nickel(II) complexes of tridentate N_3 ligands. *Inorganica Chimica Acta* **2021,** *526*, 120515, https://doi.org/10.1016/j.ica.2021.120515.
33. Al-Adilee, K.J.; Kyhoiesh, H.A.K. Preparation and identification of some metal complexes with new heterocyclic azo dye ligand 2-[2 - (1- Hydroxy -4- Chloro phenyl) azo]-imidazole and their spectral and thermal studies. *Journal of Molecular Structure* **2015,** *1137*, 160- 178, https://doi.org/10.1016/j.molstruc.2017.01.054.
34. Nagesh-Gunavanthrao, Ywernale.; Bennikallu-Hire, Mathadamrutyunjayaswamy. Metal (II) Complexes of Donor Schiff Base Ligand As A New Class Of Bioactive Compounds Containing Indole Core: Synthesis And Characterisation. *Int J Pharm Pharm Sci* **2016,** *8*, 197-204.
35. Alaghaz, A.M.A.; Ammar, Y.A.; Bayoumi, H.A.; Aldhlmani, S.A. Synthesis, spectral characterization, thermal analysis, molecular modeling and antimicrobial activity of new potentially N_2O_2 azo-dye Schiff base complexes. *Journal of Molecular Structure* **2014,** *1074*, 359-375, http://dx.doi.org/10.1016/j.molstruc.2014.05.078.
36. Mahmoud, W.H.; Deghadi, R.G.; Mohamed, G.G. Preparation, geometric structure, molecular docking thermal and spectroscopic characterization of novel Schiff base ligand and its metal chelates. *J Therm Anal Calorim* **2017,** *127*, 2149-2171, https://doi.org/10.1007/s10973-016-5826-7.
37. Mahmoud, W.H.; Omar, M. M.; Sayed, F.N. Synthesis, spectral characterization,thermal, anticancer and antimicrobial studies of bidentate azo dye metal complexes. *J Therm Anal Calorim* **2016,** *124*, 1071–1089, https://doi.org/10.1007/s10973-015-5172-1.

38. El-Ghamry, H.A.; Shaimaa Fathalla, K.; Mohamed, Gaber. Synthesis, structural characterization and molecular modelling of bidentate azo dye metal complexes: DNA interaction to antimicrobial and anticancer activities. *Appl Organometal Chem* **2017,** *32*, 4136, https://doi.org/10.1002/aoc.4136.
39. Mozhgan, Parsaei.; Zahra, Asadi.; Saeid, Khodadoust. A sensitive electrochemical sensor for rapid and selective determination of nitrite ion in water samples using modified carbon paste electrode with a newly synthesized cobalt(II)-Schiff base complex and magnetite nanospheres. *Sensors and Actuators B* **2015,** *220*, 1131–1138, http://dx.doi.org/10.1016/j.snb.2015.06.096.
40. Yuvaraj, Haldorai.; Jun-Yeong, Kim.; Ezhil-Viliana, A.T.; Nam-Su, Heo.; Yun-Suk, Huh.; Young-Kyu Hana. An enzyme-free electrochemical sensor based on reduced graphene oxide/Co3O4 nanospindle composite for sensitive detection of nitrite. *Sensors and Actuators B* **2016,** *227*, 92–99, http://dx.doi.org/10.1016/j.snb.2015.12.032.
41. Vinitha, Mariyappan.; Shen-Ming, Chen.; Keerthi, Murugan.; Alagan, Jeevika,; Tharini, Jeyapragasam,; Rasu, Ramachandra. Electrochemical sensor based on cobalt ruthenium sulfide nanoparticles embedded on boron nitrogen co-doped reduced graphene oxide for the determination of nitrite. *Colloids and Surfaces A: Physicochemical and Engineering Aspects* **2022,** *637*, 128271, https://doi.org/10.1016/j.colsurfa.2022.128271.
42. Wang, Y.N.; Wu, Y.Y.; Yang, X.Q.; Li, L.H.; Qi, B. Optimization of Nitrite Reductase Production Conditions in Lactobacillus plantarum from Salted Fish, *Adv Mater.Res* **2013,** *781-784*, 1595–1598, https://doi.org/10.4028/www.scientific.net/amr.781-784.1595.
43. Hafiza-Ammara, Naseem.; Tariq, Aziz.; Habib-ur-Rehman, Shah.; Khalil, Ahmad.; Sajidah, Parveen.; Muhammad, Ashfaq. Rational Synthesis and Characterization of Medicinal Phenyl Diazenyl-3-Hydroxy-1H-Inden-1-One Azo Derivatives and Their Metal Complexes. *Journal of Molecular Structure* **2020,** *1227*, 129574, doi: https://doi.org/10.1016/j.molstruc.2020.129574.
44. SunilKumar, N.; Krishnamurthy, G.; Somegowda, M.; Malathesh, Pari.; Ravikumar, Naik.; Jithedra Kumara, K.S.; Satheesh, Naik.; Kandagalla.; Nagaraja, Naik. Synthesis, characterization, electrochemistry, biological and molecular docking studies of the novel Co(II), Ni(II) and Cu(II) complexes derived from methanethiol bridged (2-((1H-benzo[d]imidazol-2-yl)methylthio)-1Hbenzo[d]imidazol-6-yl)(phenyl)methanone. *Journal of Molecular Structure* **2020,** *1220*, 128586, https://ui.adsabs.harvard.edu/abs/2020JMoSt122028586S/abstract.
45. Jyotimaya, sahoo.; Gulistan, parween.; Suprava, sahoo.; Suman, kumar Mekap.; Sabuj, sahoo.; Sudhir kumar, paidesetty. Synthesis ,spectral characterization,of in silico and in vitro antimicrobial investigations of some schiff base metal complexes derived from azo salicyladehyde anlogogues. *Indian journal of chemistry* **2016,** *55*, 1267-1276, http://nopr.niscair.res.in/handle/123456789/35629.
46. Ambhure, R.U.; Mirgane, S.R..; Thombal, D.U.; Shisodia, S.U. ; Pandule, S.S.; László Kótai.; Pawar, R.P. Synthesis and Antimicrobial Activity of Imines and Their Metal Complexes. *Eur. Chem. Bull* **2016,** *5*, 428-430.
47. Sunil, S.V.; Kerima, O.Z.; Santosh-Kumar, H.S.; Prabhakar, B.T.; Pramod, S.N.; Niranjana, P. In Silico Characterization of a Transcript Code Based Screening of Antimicrobial Peptide from Trichogramma chilonis. *International Joutnal of peptide and Therapeutics* **2021,** *27*, 2861-2872, https://doi.org/10.1007/s10989-021-10295-9.
48. Rauf, A.; Shah, A.; Munawar, K.S.; Khan, A.A.; Abbasi, R.; Yameen, M.A.; Khan, A.M.; Khan, A.R.; Qureshi, I.Z.; Kraatz, H.B.; Zia-ur-Rehman. Synthesis, spectroscopic characterization, DFT optimization and biological activities of Schiff bases and their metal (II) complexes. *Journal of Molecular Structure* **2017,** *1145*, 132-140, https://doi.org/10.1016/j.molstruc.2017.05.098.
49. Paresh, Debnath.; Keisham-Surjit, Singh.; Thokchom-Sonia, Devi.; Sureshkumar-Singh, S.; Butcher, R.J.; Lesław Sieroń.; Waldemar, Maniukiewicz. Synthesis, characterization, crystal structures and antidiabetic activity of organotin (IV) complexes with 2-(4-hydroxynaphthylazo)-benzoic acid. *Inorganica Chimica Acta* **2020,** *510*, 119736, https://doi.org/10.1016/j.ica.2020.119736.
50. May Juda Kareema.; Abbas Ali Salih Al-Hamdani.; Young Gun Ko.; Wail Al Zoubi Saad.; Mohammed, G. Synthesis, characterization, and determination antioxidant activities for new Schiff base complexes derived from 2-(1H-indol-3-yl)-ethylamine and metal ion complexes. *Journal of Molecular Structure* **2021,** *1231*, 129669, https://doi.org/10.1016/j.molstruc.2020.129669.
51. Fevzi Topal. Anticholinergic and antidiabetic effects of isoeugenol from clove (Eugenia caryophylata) oil. *International Journal of Food Properties* **2019,** *22*, 583-592, https://doi.org/10.1080/10942912.2019.1597882.

52. Lhami Gulcin.; Parham Taslimi.; Ayenur Aygun.; Nastaran Sadeghian.; Enes Bastem.; Omer Irfan Kurfrevioglu.; Fikret Turkan .; Fatih Sen. Antidiabetic and antiparasitic potentials: Inhibition effects of some natural antioxidant compounds on a'glycosidase, a'amylase and human gultathione S'transferase enzymes. *International Journal of Biological Macromolecules* **2018,** *119*, 741-746, https://doi.org/10.1016/j.ijbiomac.2018.08.001.
53. Nirmal Joshi.; Vishnu Gore.; Sunil Tekale.; Rajesh Nawale.; Dhanaji Rajani.; Bembalkar.; Rajendra Pawar. Synthesis and Biological Evalution Study of New Bis-imine Ligand ans Metal complexes. *Letters in Applied NanoBioScience* **2021,** *10*, 2207-2214, https://doi.org/10.33263/LIANBS102.22072214.

Supplementary materials

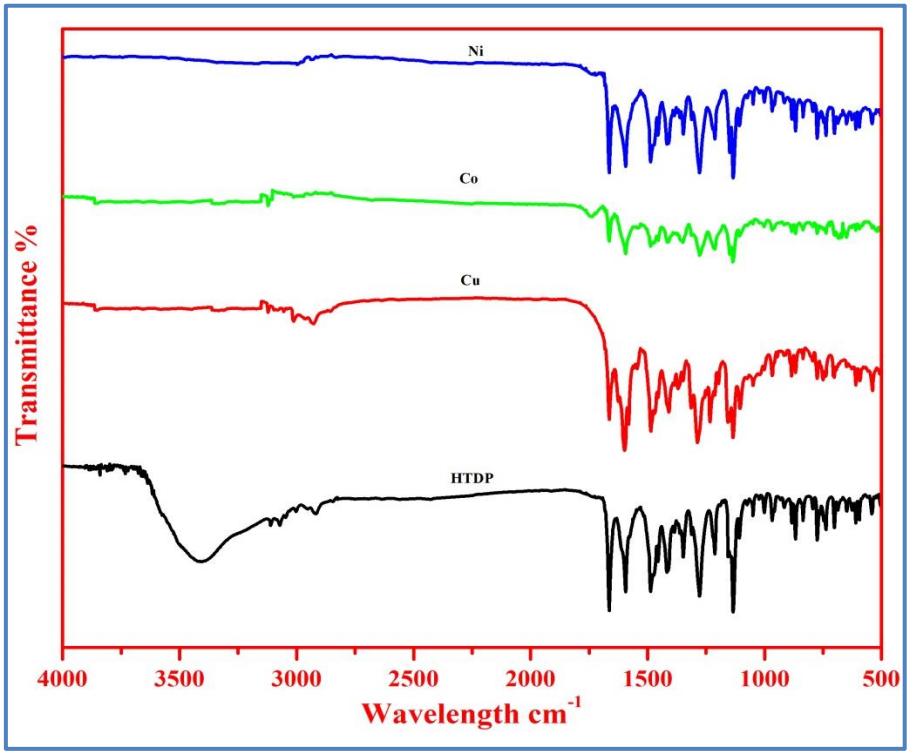

Figure S1. FT-IR spectra of synthesized compounds.

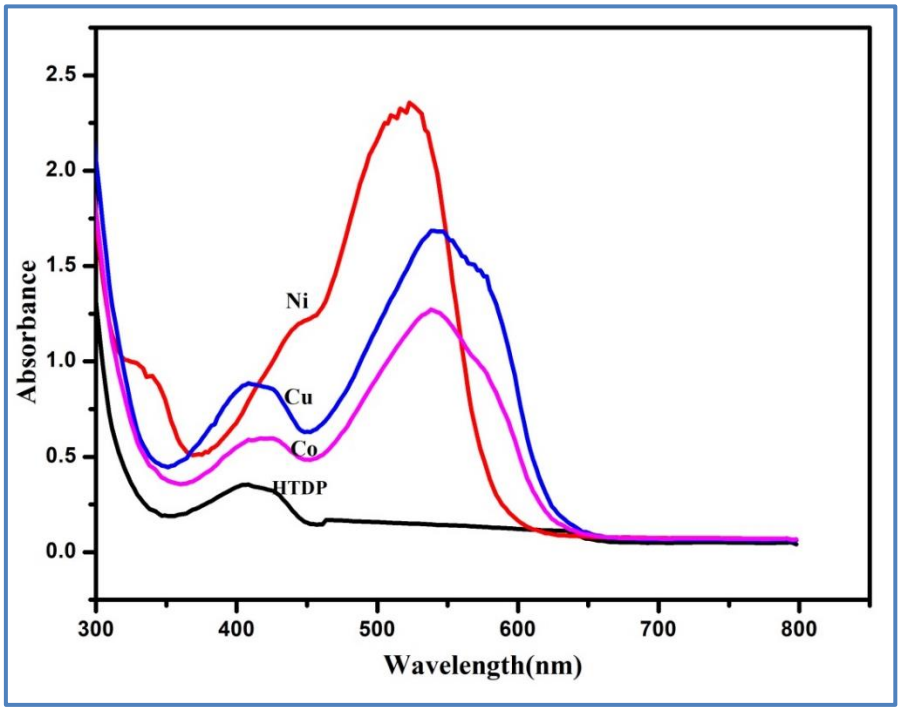

Figure S2. Electronic absorption spectra of synthesized compounds.